Progress In Electromagnetics Research C, Vol. 172, 379–391, 2026

PIER C

(Received 4 April 2026, Accepted 11 June 2026, Scheduled 18 August 2026)

Design of Ultra-Compact Multi-Band Antennas with Circular Polarization for Next-Generation IMD Applications

Vivek Gupta[1, 2, *] and Rajeev Kumar[2]

[1] *University School of Engineering & Technology, Rayat Bahra University, Mohali, Punjab, India*
[2] *Chitkara University Institute of Engineering & Technology, Chitkara University, Punjab, India*

ABSTRACT: This work presents the design and analysis of an ultra-compact multiband circularly polarised microstrip antenna for next-generation implantable medical device (IMD) applications. The antenna is constructed using a Rogers RT/Duroid 3010 substrate, characterised by a relative permittivity (εr) of 10.1 and a thickness of 0.635 mm. It features ultra-compact dimensions of $15 \times 15 \times 0.669\,\text{mm}^3$. The design allows multiband operation at frequencies 2.5 GHz, 5.8 GHz, 6.8 GHz, and 7.5 GHz. This is done by using U-shaped and rectangular slots, circular perturbations, and a modified ground structure. This configuration ensures a reflection coefficient that remains below -10 dB across both the ISM and UWB-H bands. The proposed design achieves a size reduction of approximately 25–40% compared to existing implantable antennas, while accommodating four operating bands, in contrast to conventional single- or dual-band designs. It provides enhanced bandwidth up to 9.54% in the UWB-H region. Circular polarisation is realised at higher frequencies (7.4–7.6 GHz) with an axial ratio below 3 dB, ensuring orientation-independent communication. The gain ranges from -32.2 dB to -23 dB, consistent with implantable antenna performance in lossy tissues. Performance is validated through full-wave simulations and experimental testing using a three-layer (skin-fat-muscle) tissue model. The maximum specific absorption rate (SAR) is 1.489 W/kg, averaged over 1 gram of tissue, at an input power of 1 W, meeting IEEE safety standards. Overall, this design successfully balances miniaturisation, multiband operation, polarisation performance, and safety, thereby making it suitable for dependable biomedical telemetry applications.

1. INTRODUCTION

Next-generation implantable medical devices (IMDs) require a "circularly polarised (CP)" structure of an ultra-compact multi-band microstrip antenna. These antennas enable reliable in-body wireless communication because they support various medical and ISM frequency bands in a compact enclosure. Circular polarisation increases the stability of links by minimising sensitivity to orientation, and the small size and iocompatibility allow patients to be safely ensured with reduced "specific absorption rate (SAR)" and allow integration into advanced implantable health systems. Because of their low profile, light weight, ease of manufacture, and connectivity with both planar and integrated circuits, microstrip antennas are widely used in wireless systems. Usually, a microstrip antenna is made up of a continuous ground plane on one side and a metal patch on the other side of a dielectric substance. This is a simple structure used in mobile communications, satellite networks, radar, wireless sensor networks, and IoT applications. Nevertheless, conventional microstrip antennas are limited by the following factors: narrow impedance bandwidth, single-band operation, low gain, and polarisation mismatch, and therefore cannot be used in next-generation communication applications [1].

The rapid development of wireless technologies, with increased data rates, effective spectrum management, and system miniaturisation, has generated a strong demand for advanced antenna designs. The future communication systems, such as 5G, future 6G, satellite communications, and device-to-device communications, demand antennas able to work across multiple frequency bands without compromising radiation performance. Multiband microstrip antennas have received considerable attention, since they allow the same antenna to be used to support a variety of services, thus minimizing hardware redundancy and system complexity. However, achieving multiband operation often increases design complexity or size, which is not desired in compact applications, such as smartphones and wearables.

As a result, miniaturisation has emerged as a critical requirement in antenna engineering. Ultra-compact antennas are required in space-constrained systems, such as wearable systems, unmanned aerial vehicles, small base stations, and higher integration systems such as MIMO configurations. However, reducing antenna size normally results in poor radiation efficiency, reduced bandwidth, and degraded impedance matching. Therefore, achieving compact multiband antennas without compromising performance remains a major research challenge [2].

Another consideration in design is polarisation. CP antennas have the benefits over linearly polarised antennas of low polarisation mismatch, enhanced multipath performance and robustness to changes in orientation. These properties render CP antennas very attractive to modern wireless systems. Conventional microstrip antennas are, however, naturally linearly polarised, and to become CP, it is necessary to employ other design methods, such as corner truncation, asymmetric slots, dual

* Corresponding author: Vivek Gupta (vivek.gupta@rayatbahrauniversity.edu.in).

feeding or perturbations. Circular polarisation of small multiband antennas has been especially difficult to implement but is important to provide reliable communication in next-generation systems [3, 4].

The present work addresses the issues by developing an ultra-compact multiband, CP microstrip antenna, which is specifically designed for IMD applications. The design enhances spectral efficiency, minimizes distortion, and ensures consistent performance across a range of frequency bands by optimising the antenna shape, feeding techniques, and electromagnetic behaviour. These antennas will be important in future IMD-based communication systems, including high-speed cellular networks, miniature radio-frequency (RF) front-ends, and small wireless devices.

Although modern wireless communication is based on conventional microstrip antennas, their nature limits their use, which has led to innovative design techniques, including the development of new materials and designs that will improve their performance and flexibility for various applications. This work is important in that it deals with the growing demand to develop compact, multi-band, CP antennas with the capability of reducing intermodulation effects. The results of the present research are part of the development of high-performance antenna systems that align with the high standards of next-generation IMD applications.

2. RESEARCH METHODOLOGY

Initial work on implantable medical device (IMD) antennas mainly focused on single-band operation in medically defined frequency bands, such as "Medical Implant Communication Service (MICS) band (402405 MHz)" and "Industrial, Scientific, and Medical (ISM) band (2.4248 GHz)". Traditional microstrip antennas, specifically patches and monopole types, were preferred due to their simple design and predictable radiation properties [6]. However, low frequencies required larger antenna due to longer wavelengths, which was very difficult to miniaturise. To overcome these challenges, a number of methods were invented, including utilisation of high-permittivity substrates, shorting pins, slot loading, and meandered structures. Although such strategies were successful in minimizing antennas, they tended to have low bandwidth and poor radiation efficiency [7]. As IMDs have been developed to operate in multifunctional, high-data-rate applications, the significance of multiband antenna designs has increased. Multiband operation allows using one antenna to serve many purposes, including low-power telemetry, high-speed data transfer, and wakeup signalling [8]. Many strategies have been explored to achieve multiband properties, such as slot-loaded microstrip antennas, fractal geometries, and stacked patch structures. The slot configurations, U-shaped, E-shaped, and L-shaped slots, enable the formation of more resonant modes without the need to significantly increase the size of the antenna. Fractal geometries, meanwhile, use self-similarity to create a variety of resonances with a small footprint [9].

Circular polarisation (CP) has increasing significance in implantable medical device (IMD) antennas due to its ability to overcome polarisation discrepancies caused by the random orientation and movement of devices [10, 11]. Compared to linearly polarised antennas, CP antennas provide an improved link reliability both in in-body [12] and on-body communication. Various methods have been created to realize CP in microstrip antennas, such as truncated patch corners and perturbation of slot asymmetries [13], dual-feed designs, and sequential rotation in array designs. Single-feed CP structures are also preferred in IMDs due to their lower complexity and less power consumption [14]. However, achieving a large bandwidth ratio band of compact multiband implantable antennas is a significant challenge.

The other vital consideration is the effect of the human body on antenna performance [15]. Biological tissues, which are highly permittive and conductive, play an important role in resonant frequencies, radiation efficiency, and radiation patterns. Multilayer tissue phantoms and anatomical models are popular in full-wave electromagnetic simulations to account for such effects [16, 17]. Also, encapsulation materials like polydimethylsiloxane (PDMS) and Parylene-C are not only biocompatible but also enhance impedance matching and bandwidth. These layers, however, add complexity to the design and must be optimised carefully to ensure that they meet size, performance, and safety constraints.

Another critical aspect in IMD antenna design is SAR compliance, as regulatory standards impose strict limits on electromagnetic energy absorbed by human tissues [12, 18]. Antenna miniaturisation and appropriate distribution of near-fields can minimise SAR. Ground plane modification, "electromagnetic bandgap (EBG)" structures, and "artificial magnetic conductors (AMCs)" are some of the techniques used to localize the fields to enhance radiation efficiency and keep SAR within permissible limits. Nonetheless, these techniques can increase antenna size or fabrication complexity, which can offset the advantages of smaller SAR and make the manufacturing process more complicated.

Recent advancements in optimisation techniques, including parametric methods, genetic algorithms, and machine learning-based approaches, have enabled simultaneous optimisation of antenna parameters, such as size, bandwidth, axial ratio, and SAR [10, 11]. Despite significant progress in developing compact, multiband, and circularly polarised IMD antennas, most existing designs optimise only a limited set of parameters, often at the expense of others. Achieving ultra-compact size with stable multiband operation, effective circular polarisation, and reliable performance in lossy biological environments while maintaining SAR compliance remains a key research challenge. These limitations motivate the development of advanced antenna architectures and optimisation strategies for next-generation IMD systems, where reliability, miniaturisation, and multifunctionality are essential.

3. DESIGN METHODOLOGY

3.1. Design of Multiband Antenna System

The antenna proposed is developed on a Rogers RT/duroid 3010tm substrate whose relative permittivity is 10.1, and loss tangent is 0.0035 with a thickness of 0.635 mm. The radiat-

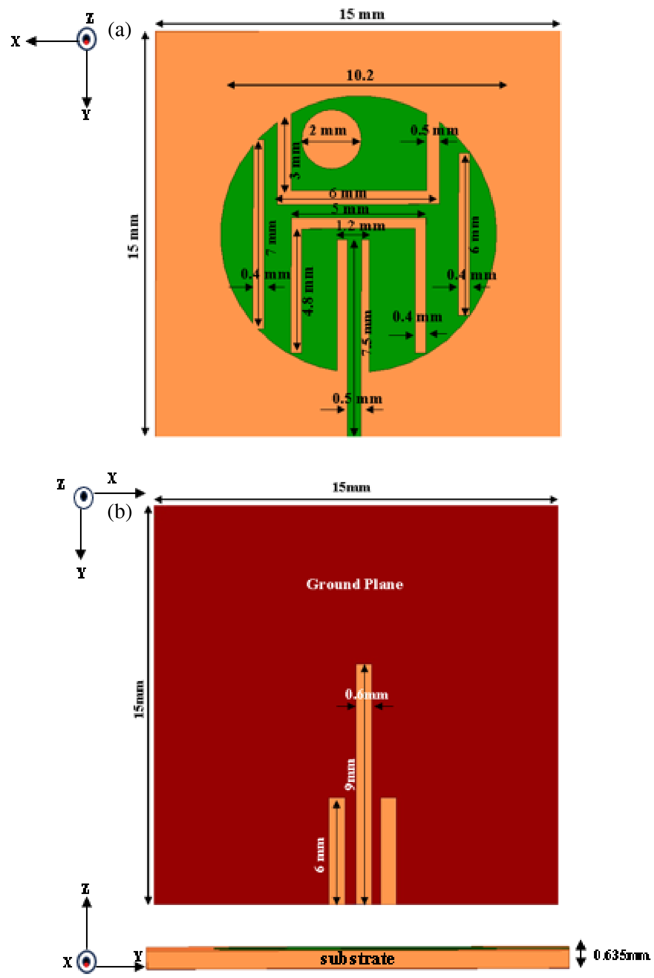

FIGURE 1. Geometry of the proposed multiband implantable antenna (unit: mm), (a) front view, (b) back view, and (c) side view.

ing patch and ground plane are modelled with copper whose thickness is 0.017 mm. The total volume of the antenna is $15 \times 15 \times 0.669\,\text{mm}^3$, which is also good to use as an implantable antenna. The antenna design relies upon a small circular patch, U-shaped slots, rectangular slots, and a circular perturbation of the radiating element. More slots are added to the ground plane to regulate current distribution and produce several resonant modes. These geometric changes are successful in making the electrical length larger than that of the physical footprint, thus allowing multiband performance.

In realistic designs of microstrip antenna, electromagnetic fields do not have complete confinement of the dielectric material, but rather, a large fraction of the field radiates in the air above the substrate as a result of fringing. Consequently, the antenna acts as a system which is in a medium with dielectric constant between those of air and substrate relative permittivity (ε_r). The parameter h is the thickness of the substrate, and D shows the effective diameter of the circular patch. Higher values of the ratio h/D improve fringing fields, resulting in increased field interaction with air and thus less ε_{eff}. The ε_{eff} parameter will be a critical concern when designing ultra-compact antennas, which, as may be seen, directly influences resonant frequency, impedance band bandwidth, and axial ratio behavior, all of which are important to attaining stable circular polarization.

$$\varepsilon_{eff} \approx \frac{\varepsilon_r + 1}{2} + \frac{\varepsilon_r - 1}{2}\left(1 + 12\frac{h}{D}\right)^{-\frac{1}{2}} \tag{1}$$

$$a_{eff} \approx \frac{F}{\sqrt{\varepsilon_{eff}}} \tag{2}$$

Patch periphery fringing fields cause the antenna's electrical size to increase compared to its physical size. This phenomenon is explained by the effective radius, which enables the resonant behavior of the antenna to be predicted correctly.

$$\text{Where } F = \frac{8.791 \times 10^9}{f_r} \tag{3}$$

where F is a frequency dependent design constant in this expression with f_r being the desired resonant frequency in hertz. This correlation makes the relationship between the frequency of operation and the size of antennas to a direct correlation. The higher the resonant frequency, the smaller the patch size, and hence antenna miniaturization is possible. The equation plays a critical role in the development of small-sized, multi-band antennas.

To verify how each structural modification contributes to multiband behavior, the antenna is developed in three stages as shown in Figure 2.

The proposed antenna is fabricated on a Rogers RO3010 substrate with dimensions $15 \times 15 \times 0.635\,\text{mm}^3$, with a relative permittivity (εr) of 10.1 and a low loss tangent ($\tan\delta = 0.0035$). Using a high-permittivity substrate enables antenna miniaturisation by electrically shortening the wavelength while maintaining acceptable radiation performance.

The radiating element contains a modified circular patch with an approximate diameter of 10.2 mm, centrally located on the substrate and incorporating multiple slots to optimise performance. The antenna is excited via a microstrip line feed, which extends from the underside of the substrate to the centre of the patch. Three aligned strip-like slots are implemented in the ground plane to enhance coupling and impedance matching.

A circular aperture on the patch functions as a parasitic resonant cavity. It disturbs the fundamental TM11 mode, helping produce higher-order resonances and providing capacitive loading that improves impedance matching at higher frequencies. The lower-frequency band is primarily produced by a U-shaped slot, lengthening the effective current path without the need to enlarge the antenna size. It also introduces inductive-capacitive loading, which improves feed coupling and return loss.

To intentionally disturb the patch's symmetry, two symmetrical vertical slots are added on either side, creating a multitude of higher-order resonances. These slots optimize the effective radiation aperture, reduce surface-wave effects, and optimize radiation stability and bandwidth at higher frequencies. The design also uses three strip-like slots in the ground plane. It has a central slot under the feed line and two shorter, symmetrical side slots. This design successfully loads the area between the

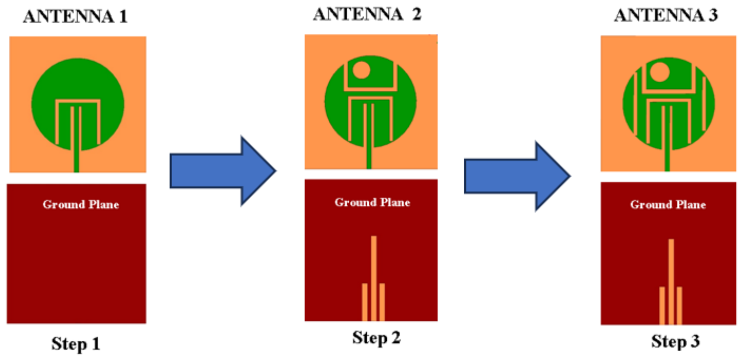

FIGURE 2. Design steps of the proposed multiband antenna.

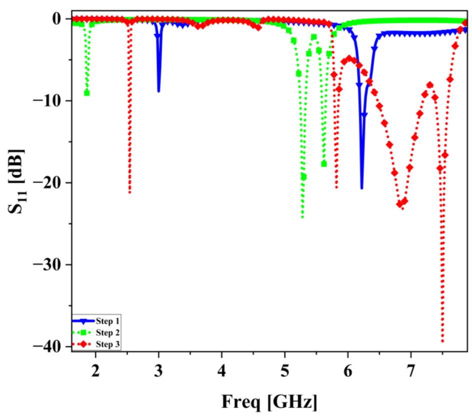

FIGURE 3. Comparison of reflection coefficient (S_{11}) results of Step 1 to Step 3 of the proposed antenna.

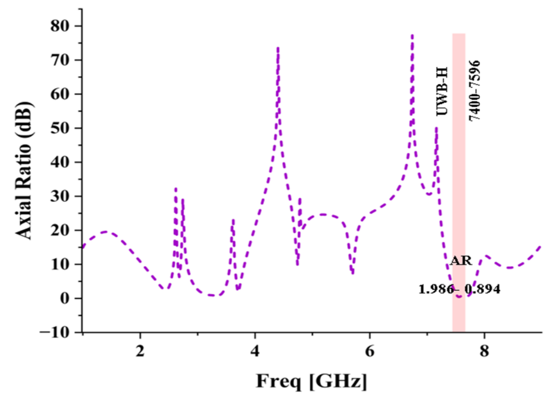

FIGURE 4. Axial ratio versus frequency, indicating circular polarization.

feed and radiating patch, leading to better impedance matching, deeper S_{11} minima, and better bandwidth. In addition, the tri-strip slots in the ground plane minimize undesired surface-wave propagation, which enhances the overall radiation efficiency. The comparison of S_{11} results of the design steps of the proposed multiband antenna is depicted in Figure 3.

The reflection coefficient (S_{11}) of the antenna in Step 1 (Figure 3) illustrates dual-band operation, with a resonance around 2.8–3.0 GHz and a stronger resonance around 6–6.3 GHz. The upper resonance is consistent with the basic TM_{11} mode of the circular patch, which is expected in theory, given the dimensions and dielectric characteristics.

A U-shaped slot is introduced to promote the emergence of the lower-frequency resonance at around 3 GHz by increasing the length of the effective current path and altering the distribution of surface currents. This change enables the use of two bands without increasing the patch's size. The S_{11} results in Step 2 suggest that the U-slot maintains the lower-frequency resonance, whereas the higher-frequency response is now two separate, sharper resonances within the 6.6–6.6 GHz range, suggesting an enhanced multiband behaviour.

This separation and amplification of high-frequency modes is achieved by introducing a circular slot, which acts as a parasitic resonant cavity with strong coupling to the dominant TM_{11} mode of the circular patch. The modified ground plane enhances this effect by introducing additional reactive loading. Consequently, this change results in better impedance matching and stronger S_{11} minima. Additional slot stabilises resonances, increases matching, and allows the designer more flexibility without increasing the antenna size. This finding confirms that the stepwise design approach is effective.

Multiband characteristics of the S_{11} response in Step 3 are considerably improved compared to the preceding steps. A good resonance is observed at 2.93–3.0 GHz, and this confirms that the lower band is due to slot-induced current extension. At higher frequencies (6–8 GHz), more distinct resonances appear instead of a single narrow mode, with a perturbation of the surface current paths by additional slots.

In comparison with Step 2, where only two high-frequency resonances are dominant, Step 3 has other modes with increased impedance, which are equivalent. The lower S_{11} minima at 6–8 GHz are a result of improved coupling between the feed and radiating element, leading to lower reflection losses and better electromagnetic performance.

In summary, the proposed antenna utilises slot loading and a modified ground plane to enable compact, multiband operation. Each slot facilitates resonance generation, impedance matching, and radiation enhancement without enlarging the antenna dimensions, thereby rendering the design well-suited for contemporary wireless and space-constrained biomedical applications. The corresponding frequency bands and bandwidths are detailed in Table 1.

TABLE 1. Achieved frequency bands with a bandwidth of the proposed multiband antenna.

Bands Achieved	Frequency (MHz)	Bandwidth Achieved (MHz)
ISM	2520–2551	31
ISM	5791–5853	62
UWB-H	6524–7173	649
UWB-H	7381–7567	186

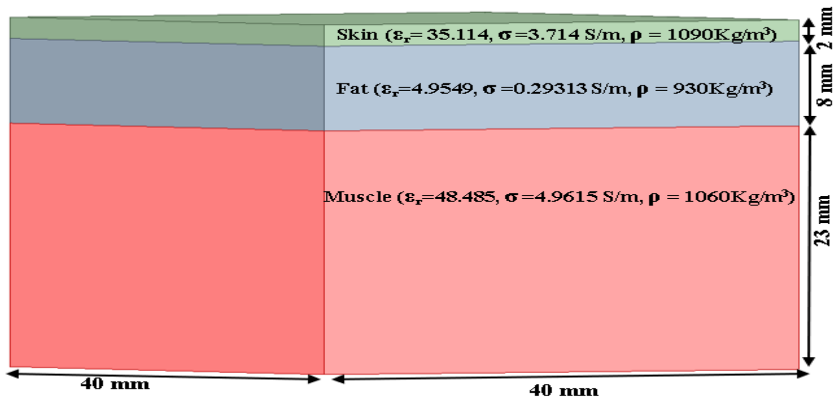

FIGURE 5. Three-layer human skin phantom.

3.2. Circular Polarization (Axial Ratio) Analysis

The plotted "axial ratio (AR)" response illustrates circular polarisation behaviour of the proposed antenna over a wide frequency range. As noted, AR varies considerably at lower frequencies, staying considerably above the 3 dB mark, meaning that the antenna radiates mostly linearly polarised waves in those areas. Several sharp peaks and variations are observed between 2 and 6 GHz, which verify the lack of stable circular polarisation in these bands. However, with increasing frequency, especially near the higher microwave region, especially near the ultra-wideband high (UWB-H) region, which is indicated between about 7.40 and 7.596 GHz, there is a significant dip in AR response.

The AR decreases below the 3 dB criterion, reaching a minimum value of about 0.894 dB near this band's central point. This clearly confirms that the antenna successfully achieves circular polarisation within this specified UWB-H band.

The limited AR bandwidth indicates that the antenna is only capable of operating as an effective circular polariser within this restricted frequency range, and beyond this range, it is mostly linearly polarised as the AR values exceed 3 dB. Consequently, Figure 4 confirms that the engineered antenna is appropriate for circularly polarised UWB-H applications within the 7.4–7.6 GHz range Figure 4.

4. SIMULATION RESULTS

A thorough parametric analysis was conducted via simulations of the proposed antenna in Step 3, as illustrated in Figure 1.

4.1. SAR Analyses for Implantable Safety

A planar three-layer tissue model of dimensions 40 mm $\times$ 40 mm $\times$ 33 mm is used for SAR evaluation, consisting of fat, skin, and muscle layers. Figure 5 shows a multilayer human body tissue model comprising of skin (2 mm), fat (8 mm), and muscle (23 mm) layers. These tissues' dielectric properties, such as permittivity, conductivity, and density, differ significantly and have a very large effect on the absorption of electromagnetic waves and power dissipation in the body. SAR is a measure of the speed at which electromagnetic energy is absorbed in per unit a mass of biological tissue, which is given as watts per kilogram (W/kg). This parameter is essential for safety, as outlined by regulatory organisations, such as IEEE C95.1 and ICNIRP. They set forth limits of 1.6 W/kg averaged over 1g of tissue according to FCC standards, or 2 W/kg averaged over 10 g of tissue per ICNIRP standards, to maintain thermal safety during the operation of implants [19].

The proposed multiband antenna is tested for each layer separately by inserting it into the layer, as shown in Figure 6. The SAR is calculated utilising $SAR = \frac{\sigma}{\rho}|E|^2$, where '$E$' (V/m) represents electric field intensity; 'σ' (S/m) indicates conductivity of human tissue; and 'ρ' (kg/m^3) reflects mass density of human tissue.

Table 2 summarizes the SAR and total gain performance of the proposed implantable antenna in different biological environments. These environments include skin, fat, muscle layers, and a skin phantom. Such parameters are highly essential in assessing safety and radiation efficiency of implantable antennas in biomedical communication.

SAR is the rate of electromagnetic energy absorption in biological tissues in watts per kilogram (W/kg) per 1 gram of tissue. Reduced SAR values signify safer operation with the

TABLE 2. Obtain SAR and Gain at different layers of skin phantom of the proposed antenna.

Layers	SAR W/kg (over 1 g of tissue)	Gain Total (dB)
Skin	0.703	−16.1
Fat	0.775	−6.2
Muscle	1.316	−29.9
Skin Phantom	1.489	−20.05

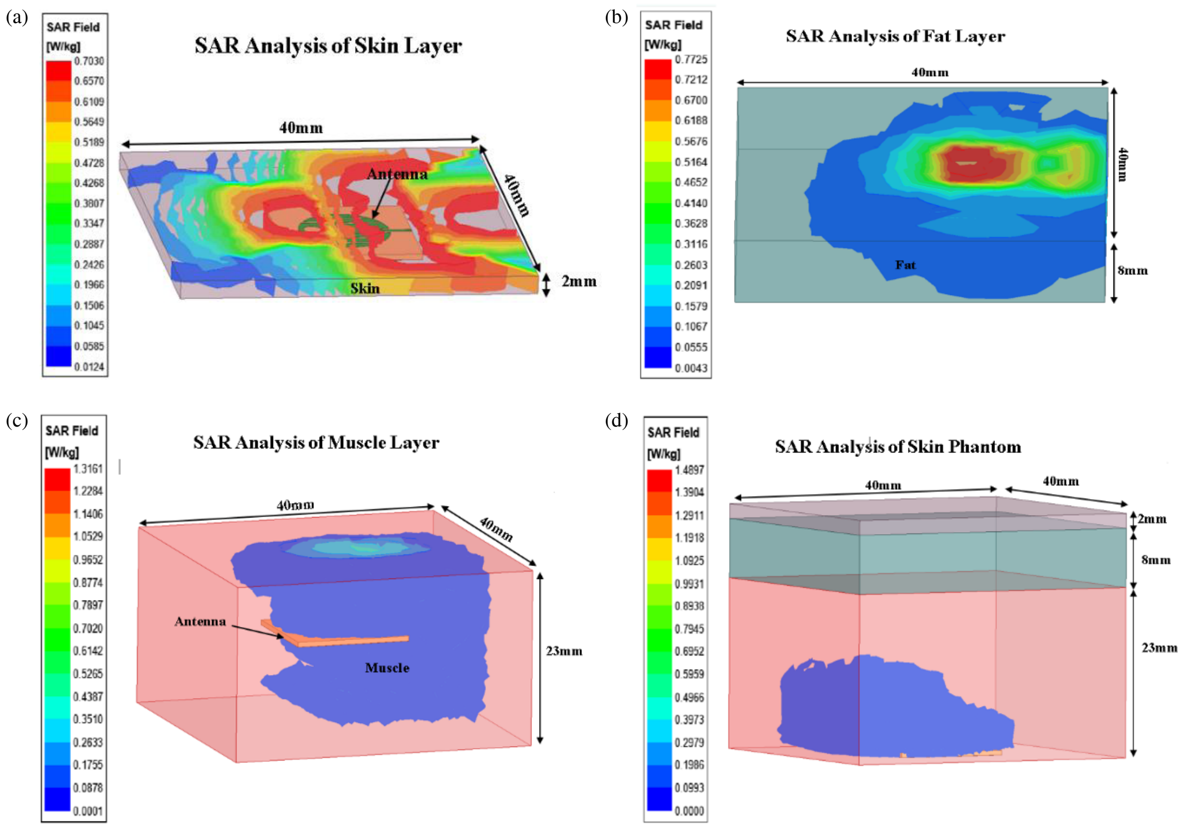

FIGURE 6. SAR analysis results for (a) skin layer, (b) fat layer, (c) muscle layer, and (d) human skin phantom.

least thermal impact, thereby meeting biomedical safety requirements. The SAR in the table are acceptable biomedical values, which confirm the antenna's suitability in implantable applications.

The muscle demonstrates, of tissue layers has a higher SAR value (1.316 W/kg) than skin and fat, due to its higher water content, conductivity, and dielectric constant, which increase electromagnetic energy absorption. The highest SAR value of 1.489 W/kg material in the skin phantom is attributed to its design that strongly resembles the characteristics of biological tissues, which may cause a somewhat higher but evenly distributed absorption in experimental validation process.

The SAR of fat tissue is relatively low (0.775 W/kg), a characteristic of low electromagnetic energy absorption ability. This is because it has low conductivity and dielectric loss which reduce its capability of absorbing RF energy; thus, it is a safer medium with improved power dissipation characteristics.

This behaviour is also supported by gain radiation characteristics in the different tissue environments illustrated in Figure 7. The greatest gain of −6.2 dB is in fat tissue, indicating that fat tissue has low-loss properties. Comparatively, the skin exhibits moderate signal attenuation, a gain of −16.1 dB, which is its intermediate dielectric characteristics. However, the gain of muscle is far less at −29.9 dB, which means that RF signals are heavily absorbed and scattered. The gain of the skin phantom is −20.05 dB; this is a negative figure, but it shows that the phantom performs quite well in controlled conditions, as it is able to simulate real-life conditions.

4.2. Influence of Bending on Conformal Surface

The antenna exhibits matching, stable impedance, and radiation properties that are not deteriorated due to bending and demonstrate conformal and implantable applications.

Figure 8 shows the proposed implantable antenna conformal testing setup, which is bent around a cylindrical surface with radius R. This design evaluates its mechanical flexibility and electromagnetic stability in realistic implantation conditions.

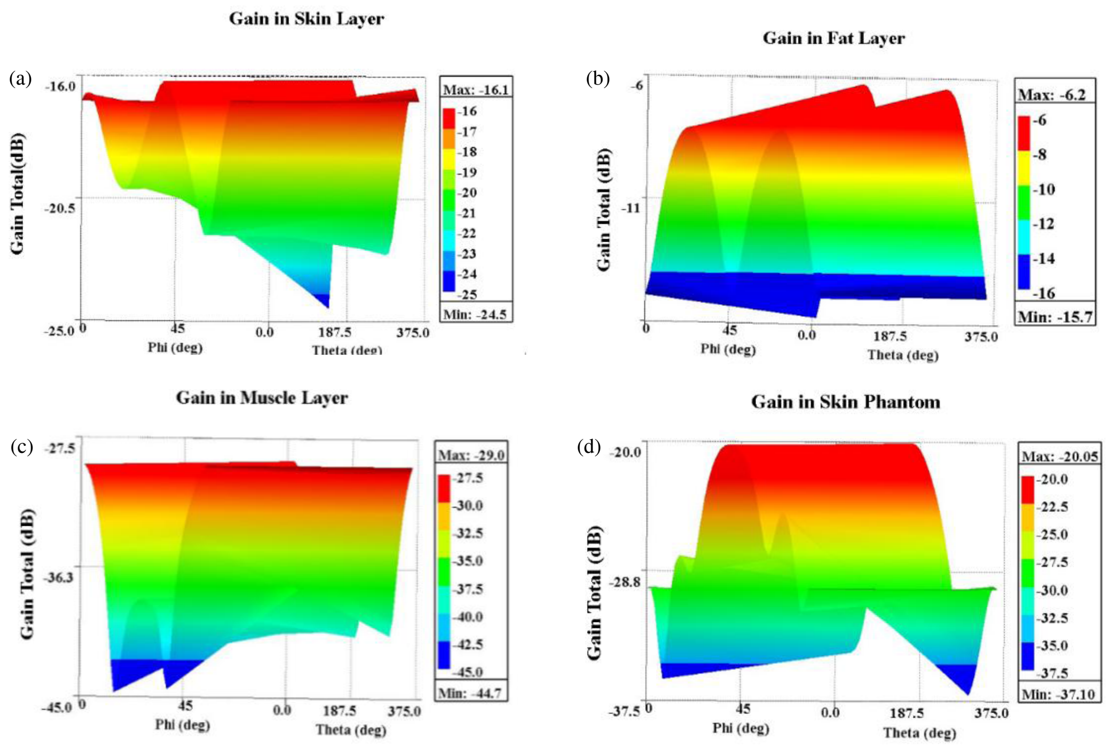

FIGURE 7. Gain in (a) skin layer, (b) fat layer, (c) muscle layer, and (d) skin phantom.

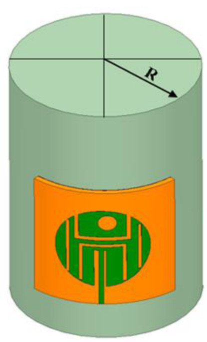

FIGURE 8. Bending of the proposed antenna.

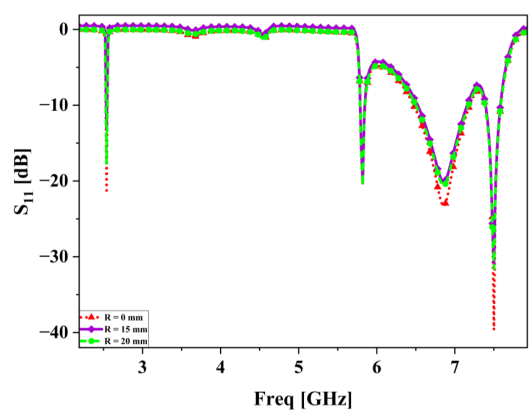

FIGURE 9. Reflection coefficient (S_{11}) results comparison under bending radii $R = 0$ mm, 15 mm, and 20 mm.

As implantable antennas are intended to operate in curved biological tissues (e.g., skin, fat, and muscle) but not a flat environment, such a conformal analysis is essential to accurate performance evaluation.

Figure 9 shows how bending influences the antenna's reflection coefficient (S_{11}) at 0 mm (flat), 20 mm, and 15 mm cylindrically radii of antenna. The study of effects of bending on impedance matching and resonant behaviour is critical since in real-world application, the antenna is matched to curved anatomical structures. This guarantees confidence in real-life biomedical applications.

In the case of the flat antenna ($R = 0$ mm), the antenna has strong, deep resonance dips at the frequencies of interest, which shows that the antenna radiates well, and the impedance is well matched, which can be used as a reference. Bending to a radius of 15 mm, the S_{11} response exhibits minor resonant frequency and magnitude changes of the dip as a result of structural deformation, which changes current distribution, electrical path length, and impedance properties. With these variations, all resonances remain below -10 dB, which suggests good matching and operational stability even in the presence of a significant curvature.

At a 20 mm bending radius, the S_{11} properties are more stable, and resonant frequencies are nearly the same as those of the flat antenna. This increased impedance matching implies that structural changes can have a small effect on performance. The S_{11} response for larger bending radii is highly similar to that of the flat antenna and shows no functionality degradation or significant detuning. This proves that the slightest bending has little influence on antenna performance. Table 3 also confirms that despite the additional bending resulting in minor frequency and S_{11} variations due to changes in current paths and electromagnetic coupling, the antenna always has an S_{11} of less

TABLE 3. Comparison of frequency and bandwidth of the proposed antenna over different bending radii.

Radius of bending	**R = 0 mm**		**R = 20 mm**		**R = 15 mm**	
Frequency Bands	Freq (MHz)	BW (MHz)	Freq (MHz)	BW (MHz)	Freq (MHz)	BW (MHz)
ISM	2520–2551	31	2529–2550	21	2533–2547	14
ISM	5791–5853	62	5787–5849	62	5789–5840	51
UWB-H	6524–7173	649	6523–7156	633	6560–7120	560
UWB-H	7381–7567	186	6466–6502	191	7400–7574	174

(a)

(b)

FIGURE 10. Prototype of proposed multiband antenna. (a) Front view and (b) back view.

than -10 dB. These findings indicate the antenna's excellent mechanical versatility and electromagnetic stability and guarantee its good performance in real-life biomedical implantation applications.

5. EXPERIMENTAL VALIDATION OF PROPOSED ANTENNA

A fabricated prototype of the proposed antenna is illustrated in Figures 10(a) & (b). The functionality of the proposed implantable antenna has been tested in an experimental configuration, as shown in Figures 11(a) and (b), using a high-precision measurement device in a realistic biological environment. This specific arrangement was carefully engineered to stimulate in-body operational parameters, thus making it easy to precisely obtain antenna reflection characteristics. Within this configuration, the antenna was interfaced with.

A skin-mimicking gel is developed to evaluate the antenna in an implanted or in vitro environment [20]. The composition includes Triton X-100, sodium chloride, vegetable oil, Gelatine A, hand soap, deionised water, and pink food colouring for visual identification. Among them, deionised water has the greatest electrical effect and vegetable oil the least; by altering their proportions, it is possible to simulate varying water content in human soft tissues.

Adding sodium chloride makes the material more conductive and lowers its relative permittivity. This causes permittivity to drop quickly from 500 MHz–1 GHz and slowly from 1GHz to 20 GHz [21, 22]. Other components, such as gelatine A, Triton X-100, hand soap, and colouring, have minimal impact due to their low concentrations. These variations allow accurate emulation of different human tissues, with Table 4 listing the component percentages.

TABLE 4. Ingredients for skin-mimicking material.

S. No.	**Ingredients**	**Percent volume**
i	Deionised Water	68.33
ii	Vegetable Oil	20.68
iii	Gelatine A	8.99 ($\rho = 1.2\,\mathrm{g\,ml^{-1}}$)
iv	Soap	0.899
v	Triton X-100	0.899
vi	Sodium Chloride	0.166 ($\rho = 2.165\,\mathrm{g\,ml^{-1}}$)
vii	Pink food colouring	0.037 (1 drop = 0.042 ml)

Figure 12 is an analysis of simulated and realized reflection coefficients (S_{11}) of the proposed ultra-compact multiband microstrip antenna in free space. Several distinct resonant bands can be seen at 2.6 GHz, 6.0 GHz and 7.5 GHz, indicating multi-band functionality. The calculated values are in very close agreement with the simulated values with slight deviations due to fabrication tolerances and connector losses. The S_{11} response exhibits deep minima below -10 dB, indicating good impedance matching and effective radiation performance. This shows that the antenna has efficient radiation behavior and compatibility in its design with the next-generation circularly polarized IMD.

Figure 13 shows a comparison of S_{11} in a simulation carried out in a skin phantom and a tissue sample, which is a realistic environment of implantable devices. Slight resonance shifts and impedance changes are due to the lossy, high-permittivity

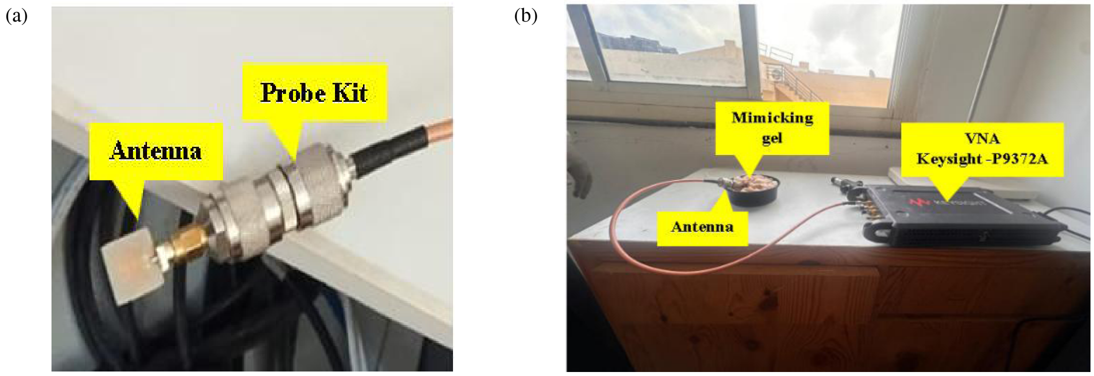

FIGURE 11. Fabricated prototype testing environment using VNA. (a) Free space and (b) mimicking gel.

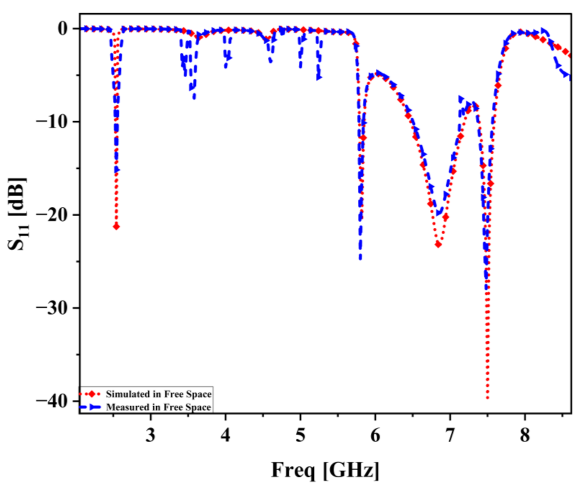

FIGURE 12. Comparison of reflection coefficient (S_{11}) results in free space.

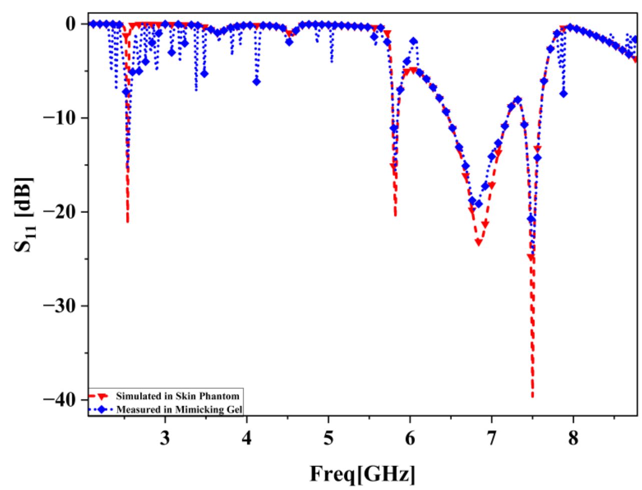

FIGURE 13. Comparison of reflection coefficient (S_{11}) results in skin phantom and mimicking gel.

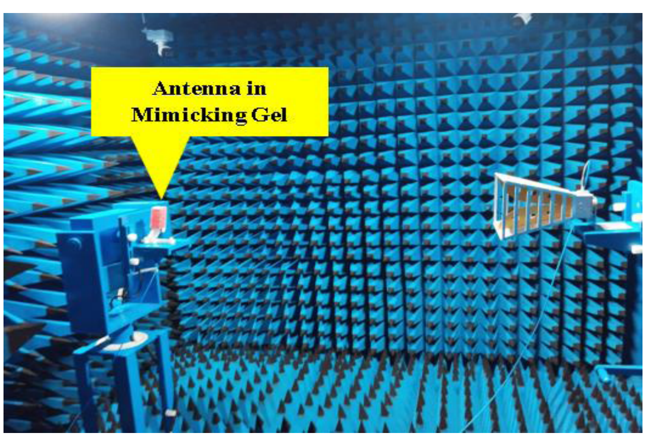

FIGURE 14. Antenna prototype measurement setups in an anechoic chamber.

biological environment. In spite of this detuning, the antenna still has several resonant bands with high matching ($S_{11} < -10$ dB). The high consensus confirms the design robustness, consistent stable circular polarisation and performance, which proves its appropriateness in the communication of implantable medical devices in human tissues.

5.1. Radiation Pattern Analysis

Figure 14 shows the radiation measurement setup of the proposed antenna in an anechoic chamber. The antenna is inserted into the tissue-mimicking gel to simulate an actual implant. Absorbing walls of the anechoic chamber reduce reflections, thereby enabling accurate gain and radiation-pattern characterization. These measurements provide an assessment of the antenna's radiation performance and polarization characteristics under realistic in-body conditions.

Figure 15 shows the total gain radiation patterns at different resonant frequencies. Red and blue dashed curves represent the two orthogonal field components. Usually, the patterns show omnidirectional characteristics with low peak gain, which is normal for implantable antennas because the tissue absorbs signals.

This design allows the device to communicate reliably, regardless of its position within the body. At 2520 MHz, the E-field pattern in Figure 15(a) shows nearly omnidirectional behaviour, with a broad main lobe indicating a uniform current distribution. Conversely, the symmetrical H-field pattern in Figure 15(b) indicates a balanced field distribution, supporting the stable circular-polarization characteristics of the antenna. The E-field in Figure 15(c) at 5791 MHz is more direc-

TABLE 5. Comparison of gain for measured and simulated values.

Band	Gain Simulated (dB)	Gain Measured (dB)
ISM (2520–2551)	−37	−23
ISM (5791–5853)	−34	−34.5
UWB-H (6524–7173)	−27	−32.1
UWB-H (7381–7567)	−22.4	−32.2

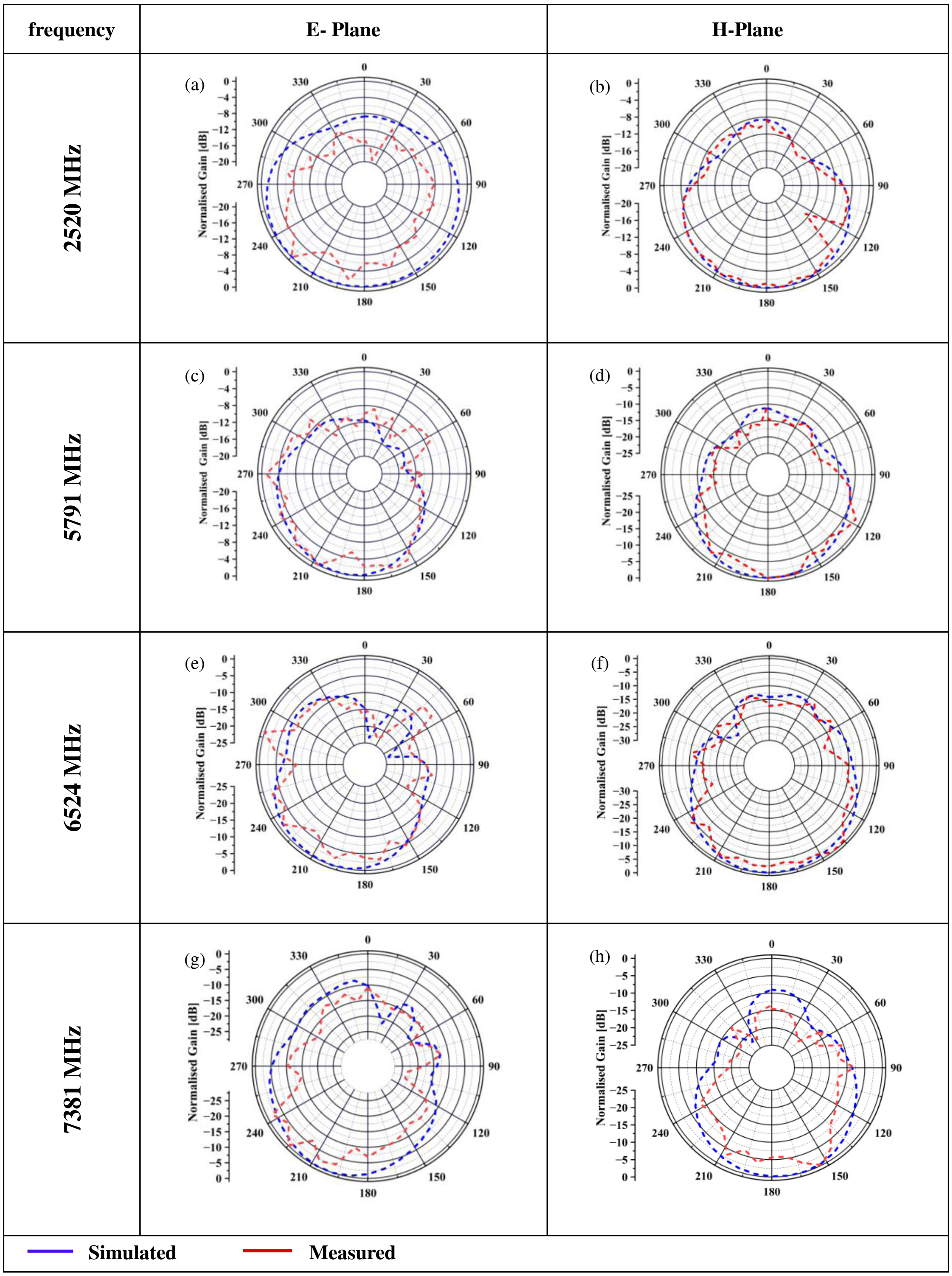

FIGURE 15. Radiation pattern in E and H plane at 2520 MHz, 5791 MHz, 6524 MHz, and 7381 MHz.

TABLE 6. Comparison of parameters for various antennas from various studies.

Reference	Operating Bands (GHz)	Size (mm^3)	Polarization	Peak Gain (dB)	Bandwidth (%)	Axial Ratio (dB)	SAR (W/kg)
Ref. [2]	0.403	576	Linear	−28	1.2	—	1.45
Ref. [5]	0.403, 2.45	216	Linear	−30, −18	1.5, 4.1	—	1.62
Ref. [8]	0.915, 2.45	196	Linear	−25, −16	2.3, 5.0	—	1.58
Ref. [9]	0.403, 1.4, 2.45	152	Circular (Higher freq band)	−27, −20	1.8, 3.9	< 3	1.41
Ref. [10]	1.4, 2.45	150	Circular	−22, −15	3.2, 6.5	< 3	1.36
Ref. [15]	0.403, 2.45, 3.5	64	Circular (Higher freq band)	−24, −14	2.0/5.8	< 2.5	1.29
Ref. [23]	0.405, 2.48	798	Linear	−331, −14.55	38.1, 17.6	—	0.708, 1.497
Ref. [24]	0.608, 1.432	536	Linear	−26.5, −19.9	16.3, 10.6	—	1.59
Ref. [25]	0.397, 2.49	1026	Linear	−20.02, −22.82	9.4, 8	—	1.5
Ref. [26]	0.402, 2.45, 2.95	528	Linear	−29.7, −3.1, −7.3		—	1.24, 1.45, 1.8
Ref. [27]	0.444, 1.644	604.8	Linear	−46.5, −28.2	90.9, 53.7	—	0.489, 1.19
Ref. [28]	1.450, 2.450	960	Linear	−32, −36	36	—	0.907, 1.11
Ref. [29]	0.400, 2.4 GHz, 5.7 GHz	524.4	Linear	−40, −15, −13.5	13.25, 9.69, 6.27	—	0.494, 0.344, 0.320
Proposed work	**2.5, 5.8, 6.8, 7.5**	**150.5**	**Circular (Higher freq band)**	−22, −34.5, −32.1, −32.2	1.24, 1.07, 9.54, 2.48	< 3	**1.489**

tional and has fewer sidelobes because of higher-order modes, whereas the H-field in Figure 15(d) is balanced, preserving the purity of polarisation and enhancing the gain. The E-field in Figures 15(e)–(f) at 6524 MHz shows higher directivity and controlled sidelobes, which is an indication of successful multi-band excitation. The H-field, on the other hand, maintains its angular coverage. At 7381 MHz, the E-field in Figure 15(g) is highly directive, and the symmetrical H-field in Figure 15(h) reaffirms consistent performance and stable circular polarisation, making it suitable for implantable medical devices.

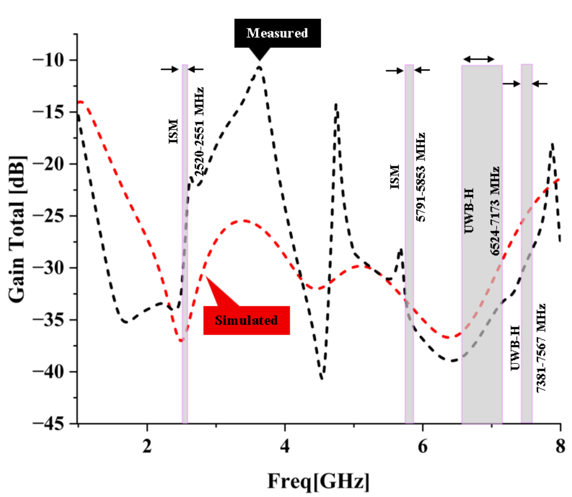

FIGURE 16. Gain comparison for measured and simulated values.

Figure 16 shows a comparison between simulated and measured gains versus frequency of the proposed implantable antenna. The antenna operates on ISM (2.520–2.551 GHz and 5.791–5.853 GHz) and UWB-H (6.524–7.173 GHz and 7.381–7.567 GHz). There is close consistency between measured and simulated data, as shown in Table 5. The slight deviations are due to fabrication tolerances and tissue-loading effects, which verify credible multiband radiation functionality when applicable in IMD applications.

Firstly, in terms of size, the proposed antenna (150.5 mm^3) is significantly compact compared to many reported designs such as [23], [25], and [28] while still maintaining competitive performance. This reflects the efficient miniaturisation achieved without severely degrading radiation characteristics.

Secondly, most earlier designs operate on only one or two frequency bands, mainly the MICS band (around 0.4 GHz) and ISM band (2.45 GHz). The proposed design, on the other hand, operates on four frequency bands (2.5, 5.8, 6.8, and 7.5 GHz), and it enables more advanced features, including high data-rate communication and more compatibility with modern biomedical telemetry systems. Such multiband capability is a definite advancement over previous works. Polarisation-wise, most of the reference antennas are linearly polarised and therefore subject to polarisation mismatch losses within the human body. The proposed antenna employs circular polarisation (CP) in higher frequencies (axial ratio < 3 dB) to achieve much better link reliability and orientation insensitivity, a significant benefit in implantable applications.

Considering gain, even though implantable antennas have low gain as a consequence of tissue losses, the proposed design offers similar performance (-22 dB to -34.5 dB range) to other works. Some of the designs are marginally better at certain bands, but tend to trade off size or bandwidth. Regarding bandwidth, the proposed antenna attains sufficient fractional bandwidths in various bands and matches or exceeds a few previous works with very limited bandwidths (e.g., $\sim$ 1–3 percent). This guarantees that it works more steadily in detuning conditions in biological tissues. Lastly, regarding SAR, the suggested antenna will have a value of 1.489 W/kg, which does not exceed the IEEE safety limit (1.6 W/kg of 1 g tissue). This proves that the antenna is safe to implant in biomedical devices, despite the multiband and compact design, which is as safe as most reported references.

Overall, the proposed work has a good trade-off among miniaturisation, multiband functionality, circular polarisation, and safety compliance, which is not simultaneously achieved in most of the compared designs, as shown in Table 6. This confirms its excellence and ability to be utilised in contemporary implantable medical devices.

6. CONCLUSION AND FUTURE SCOPE

The current study focuses on the design of an ultra-compact multi-band CP microstrip antenna which can be used in next-generation Implantable Medical Devices (IMDs). These devices should meet high requirements, such as size, safety, and effective communication. The antenna is designed on a high-permittivity Rogers RT/Duroid 3010 substrate ($\varepsilon r = 10.1$, thickness $= 0.635$ mm, and loss tangent $= 0.0035$), allowing it to reduce size considerably and still achieve acceptable electromagnetic performance. It is small in size with a total volume of $15 \times 15 \times 0.669\,\text{mm}^3$ and can play a role in areas with space constraints in implants. The radiating patch has U-shaped, rectangular, and circular holes, which enable multiband operation by exploiting multiple resonant modes. Additionally, three slots are incorporated into the ground plane to improve impedance bandwidth and radiation stability in lossy biological environments. A microstrip line inset-fed is optimised to achieve the desired impedance matching and reflection coefficients less than -10 dB at 2.5 GHz, 5.8 GHz, 6.8 GHz and 7.5 GHz in the ISM and UWB-H bands.

At higher frequencies, circular polarisation is achieved by the controlled perturbation of orthogonal surface currents, realising an axial ratio below 3 dB and minimising polarisation mismatch due to the implant orientation and body motion. Simulation and measurement outcomes confirm stable radiation properties, in which gain is around -23 dB at lower frequencies to -32.2 dB at higher frequencies, indicating good signal propagation in biological tissues. A three-layer (skin, fat, muscle) tissue model safety validation demonstrates a maximum SAR of 1.489 W/kg (average of 1 g), within the IEEE safety limits, and is biocompatible.

In spite of these advancements, more effort is required to enhance bandwidth and radiation efficiency at lower medical frequencies without the need to increase the antenna. Future studies can explore magneto-dielectric substrates, flexible biocompatible materials and meta surface-based miniaturisation methods. Furthermore, experimental validation using anatomically accurate phantoms could help bridge the gap between simulation and practical implantation.

REFERENCES

[1] Qamar, M., K. Y. Kapusuz, L. Carslake, T.-H. Loh, M. A. Thaha, and A. Alomainy, "Ultra-compact camera-integrated deep-implanted two-port mimo antenna for high-data-rate wireless capsule endoscopy," *IEEE Journal of Electromagnetics, RF and Microwaves in Medicine and Biology*, Vol. 9, No. 3, 293–301, 2025.

[2] Basir, A., Y. Cho, I. A. Shah, S. Hayat, S. Ullah, M. Zada, S. A. A. Shah, and H. Yoo, "Implantable and ingestible antenna systems: From imagination to realization [bioelectromagnetics]," *IEEE Antennas and Propagation Magazine*, Vol. 65, No. 5, 70–83, 2023.

[3] Sundaravadivel, P., S. Thangavel, G. B. P. Jegajothi, R. Meenakshi, D. S. S. Raja, and D. R. Kumar, "A high-performance, thin, circularly polarized microstrip antenna for compact radar systems," *Progress In Electromagnetics Research Letters*, Vol. 124, 31–36, 2025.

[4] Singh, D., N. Kashyap, and A. Thakur, "Design and optimization of a hexagonal-slotted wideband microstrip antenna for 5 G networks RF energy harvesting," *Franklin Open*, Vol. 13, 100409, 2025.

[5] Sharma, M., P. R. Kapula, S. Salagrama, K. Sharma, G. P. Pandey, D. K. Singh, M. Mahajan, and A. Gupta, "Miniaturized quad-port conformal multi-band (QPC-MB) MIMO antenna for on-body wireless systems in microwave-millimeter bands," *IEEE Access*, Vol. 11, 105 982–105 999, 2023.

[6] Al-Tumah, W. A. G., R. M. Shaaban, and A. P. Duffy, "Design, simulation, and fabrication of a double annular ring microstrip antenna based on gaps with multiband feature," *Engineering Science and Technology, an International Journal*, Vol. 29, 101033, 2022.

[7] Rahman, A. A. M., M. T. Islam, M. Moniruzzaman, S. K. A. Rahim, M. Singh, N. Misran, M. S. Islam, and M. S. Soliman, "H-shaped modifiers loaded mirror symmetric resonator based double negative metamaterial for multi-band wireless communications," *Scientific Reports*, Vol. 13, No. 1, 15943, 2023.

[8] Asgharivaskasi, R., V. Mashayekhi, N. Azadi-Tinat, and M. Koohestani, "Ultra-compact quad-band half-mode SIW bandpass filter for Sub-6 GHz 5G applications," *Scientific Reports*, Vol. 15, No. 1, 30077, 2025.

[9] Neamah, W. A., H. M. A. Sabbagh, and H. Al-Rizzo, "A compact two-element linearly and orthogonal circularly polarized MIMO antenna system for 5G cellular and WLAN/Wi-Fi 6E application," *IEEE Access*, Vol. 11, 96 879–96 891, 2023.

[10] Patel, D. H. and G. D. Makwana, "Multiband antenna for 2G/3G/4G and sub-6 GHz 5G applications using characteristic mode analysis," *Progress In Electromagnetics Research M*, Vol. 115, 107–117, 2023.

[11] Sharma, M., K. Sharma, P. R. Kapula, A. Nayyar, and M. Bilal, "Dual-Wide Multi-Band (DWMB) four-port flexible MIMO antenna for on-body multiple wireless applications including high diversity performance," *PLoS ONE*, Vol. 19, No. 11, e0309690, 2024.

[12] Song, Z., D. Yang, Y. Wang, Y. Shi, X. Zheng, and L. Wang, "A compact circularly polarized ultra-wide bandwidth implantable antenna for multiple scenarios," *Scientific Reports*, Vol. 16,

3139, Jan. 2026.

[13] Himavanth, N., M. Arshad, S. Kumaravel, R. Natarajan, A. Chandra, and M. Karthikeyan, "Compact circle-shaped circularly polarized implantable antenna with combined E and hexagonal shaped patch for wireless biotelemetry," *Results in Engineering*, Vol. 27, 105758, 2025.

[14] Yin, B., M. Ye, J. Cong, and Y. Xu, "A miniaturized dual-band circularly polarized implantable antenna by half-cutting," *Progress In Electromagnetics Research M*, Vol. 108, 139–149, 2022.

[15] Sharma, D., R. Kumar, and R. K. Vishwakarma, "A miniaturized dual-band modified rectangular-shaped antenna for wireless applications," *International Journal of Electrical and Electronics Research*, Vol. 10, No. 4, 877–880, 2022.

[16] Altakhaineh, A. T., S. S. Alja'afreh, A. M. Almatarneh, E. Almajali, L. Al-Tarawneh, and J. Yousaf, "A quad-band shared-aperture antenna based on dual-mode composite quarter-mode SIW cavity for 5G and 6G with MIMO capability," *Electronics*, Vol. 12, No. 11, 2480, 2023.

[17] Sharma, D., B. K. Kanaujia, V. Kaim, R. Mittra, R. K. Arya, and L. Matekovits, "Design and implementation of compact dual-band conformal antenna for leadless cardiac pacemaker system," *Scientific Reports*, Vol. 12, No. 1, 3165, 2022.

[18] Dayo, Z. A., Q. Cao, Y. Wang, P. Soothar, I. A. Khoso, G. Shah, and M. Aamir, "A compact high gain multiband bowtie slot antenna with miniaturized triangular shaped metallic ground plane," *Applied Computational Electromagnetics Society*, Vol. 36, No. 7, 935–945, 2021.

[19] Hu, X.-y., W.-l. Yin, F. Du, C. Zhang, P. Xiao, and G. Li, "Biomedical applications and challenges of in-body implantable antenna for implantable medical devices: A review," *AEU — International Journal of Electronics and Communications*, Vol. 174, 155053, 2024.

[20] Green, R. B., M. V. Smith, and E. Topsakal, "In vitro and in vivo testing of implantable antennas," in *Antenna and Sensor Technologies in Modern Medical Applications*, 145–189, 2021.

[21] Gabriel, C., S. Gabriel, and E. Corthout, "The dielectric properties of biological tissues: I. Literature survey," *Physics in Medicine & Biology*, Vol. 41, No. 11, 2231–2249, 1996.

[22] Gabriel, C., "Compilation of the dielectric properties of body tissues at RF and microwave frequencies," Tech. Rep., 1996.

[23] Ganeshwaran, N., J. K. Jeyaprakash, M. G. N. Alsath, and V. Sathyanarayanan, "Design of a dual-band circular implantable antenna for biomedical applications," *IEEE Antennas and Wireless Propagation Letters*, Vol. 19, No. 1, 119–123, Jan. 2020.

[24] Ung, J. and T. Karacolak, "A dual-band meandered dipole antenna for medical telemetry applications," *Progress In Electromagnetics Research C*, Vol. 63, 85–94, 2016.

[25] Salama, S., D. Zyoud, and A. Abuelhaija, "Design of a dual-band planar inverted F-L implantable antenna for biomedical applications," in *Journal of Physics: Conference Series*, Vol. 1711, No. 1, 012002, Kuala Lumpur, Malaysia, 2020.

[26] Salama, S., D. Zyoud, and A. Abuelhaija, "A compact-size multiple-band planar inverted L-C implantable antenna used for biomedical applications," *Micromachines*, Vol. 14, No. 5, 1021, May 2023.

[27] Rana, M. M., M. A. Islam, and I. M. Mehedi, "Dual-band implantable antenna loaded with patch slots for wireless biotelemetry systems," *Progress In Electromagnetics Research C*, Vol. 141, 151–162, 2024.

[28] Bahrami, S., G. Moloudian, S. R. Miri-Rostami, and T. Björninen, "Compact microstrip antennas with enhanced bandwidth for the implanted and external subsystems of a wireless retinal prosthesi," *IEEE Transactions on Antennas and Propagation*, Vol. 69, No. 5, 2969–2974, May 2021.

[29] Shahverdi, K., S. Hashemi, S. Sarafan, and H. Cao, "Triple-band implantable antenna design for biotelemetry applications in MICS/ISM/Wi-Fi/Bluetooth bands," *Technologies*, Vol. 10, No. 4, 91, Aug. 2022.